

## Quantum scattering from a sinusoidal hard wall: Atomic diffraction from solid surfaces

Richard I. Masel and Robert P. Merrill

*Department of Chemical Engineering, University of California, Berkeley, California 94720*

William H. Miller

*Department of Chemistry, University of California, Berkeley, California 94720*

(Received 9 June 1975)

An exact quantum formalism for atom scattering from a sinusoidal hard-wall surface is presented. The Lippmann-Schwinger equation is solved for a scattering kernel consistent with the hard-wall boundary conditions on the Schrödinger equation. It results in an infinite-dimensional matrix equation for the Fourier coefficients of the scattering kernel which can be solved in a finite-dimensional limit to convergence. The results show either rainbow or specular patterns depending on the surface roughness and incident  $k$  vector, as predicted by semiclassical and coupled-channel calculations. Bragg-like structure is present with the periodicity of the amplitude of the sinusoidal hard wall and the effects of multiple scattering are evidenced at large surface amplitudes.

### INTRODUCTION

The diffractive scattering of atoms from solid surfaces<sup>1</sup> played an important role in establishing the validity of quantum theory for massive particles. The use of atom scattering as a tool for the study of surface structure has developed much more slowly, however, than the use of electron scattering, i. e., low-energy-electron diffraction (LEED) and high-energy-electron diffraction (HEED). Only recently has diffractive scattering of atoms been observed for surfaces other than the alkali halides.<sup>2,3</sup> It appears as though the atomic scattering samples a repulsive potential at radii as large or larger than the interatomic spacing in solids. Thus the amplitude of the surface periodicity for many solid surfaces [e. g., the (111) planes of fcc metals] is not large enough to yield detectable diffraction intensities except for the specular beam.<sup>4</sup>

The early theory of Lennard-Jones and Devonshire<sup>5</sup> has been extended only recently to include the strong-scattering limit.<sup>6</sup> Among other modern approaches are those of Beeby, who uses a Green's-function formulation which can be solved exactly in the inelastic limit for a flat surface with a "hard wall" potential.<sup>7</sup> It has been solved only approximately, however, for a structured surface.<sup>8</sup> In an approach similar in spirit to that of Goodman *et al.*,<sup>6</sup> which appears to be the equivalent of a single scattering limit, Tshuda<sup>9</sup> and Wolken<sup>10</sup> integrate the coupled-channel equations for scattering potentials based on the Morse interaction<sup>10</sup> and the Lennard-Jones potential,<sup>9</sup> a procedure which includes multiple scattering. Levi *et al.*<sup>11</sup> have used an eikonal approximation, while Masel *et al.*<sup>12</sup> and Doll<sup>13</sup> have used the semiclassical approach which has been singularly successful in describing the gas-gas scattering of massive particles.<sup>14</sup>

In order to assess the effects of the several approximations which have been made in the modern formulation of the theory of atom scattering from solid surfaces, it would be helpful to compare the results of each method with exact multiple scattering calculations from a suitably simple scattering potential. In this paper such a calculation is presented for atomic scattering from a sinusoidal hard wall. The Lippmann-Schwinger equation<sup>15</sup> is solved for boundary conditions given by the Schrödinger equation for the hard-wall potential. For this model the formalism is exact. The only approximations are those introduced in terminating an infinite matrix whose inversion gives the coefficients needed to calculate the scattering matrix. In the results presented here the dimensionality of the "infinite" matrix is increased until numerical convergence of the scattering intensities is achieved.

The formulation is similar to Beeby<sup>7,8</sup> except that the wave function  $\psi$  is forced to be zero underneath the surface as well as within the surface contour. A sample case is also worked in order to show that setting  $\psi$  equal to zero along the surface is not sufficient.

For a completely flat surface, the model predicts purely specular scattering, but as soon as the amplitude of the surface periodicity is appreciable nonspecular diffraction peaks appear. Increasing the amplitude slightly results in a so-called rainbow pattern, where the intensity of the diffraction peaks increases slowly, moving away from specular angle until critical angles, called the rainbow angles, are reached, after which the intensity of the diffraction peaks drops off rapidly. At very large amplitudes the rainbow angles coalesce to the specular, and then appear to recede as the roughness increases. Thus, similar intensity patterns can result from two surfaces with

very different scales of periodic roughness. Qualitatively, this solution does a fairly good job of representing the main features of typical experimental scattering data. Similar features are evident in the complete coupled-channel calculations<sup>9,10</sup> and the semiclassical formulation<sup>11-13</sup> but are absent from the "single scattering" theory<sup>6</sup> and the calculations of Beeby for structured surfaces.<sup>8</sup>

### THEORY

The scattering surface is assumed to be a sinusoidal hard wall. The potential is

$$\begin{aligned} V(x, z) &= 0, & z > D(x), \\ V(x, z) &= \infty, & z \leq D(x), \end{aligned} \quad (1)$$

where  $V$  is the potential,  $z$  is the distance above the surface,  $x$  the distance along the surface, and  $D(x)$  is the surface contour.

The Lippmann-Schwinger<sup>15</sup> integral equation is a useful starting point since it contains all scattering boundary conditions explicitly. The scattering wave function  $\psi(x, z)$  is then determined by

$$\begin{aligned} \psi(x, z) &= \Phi_I(x, z) + \int_{-\infty}^{\infty} dx' \int_{-\infty}^{\infty} dz' \\ &\quad \times G_0^*(x, z; x', z') V(x', z') \psi(x', z'), \end{aligned} \quad (2)$$

where  $\Phi_I(x, z)$  is the incident wave and  $G_0^*$  is the free-particle Green's function with the usual outgoing boundary conditions. Defining  $F(x, z)$  by

$$F(x, z) \equiv V(x, z) \psi(x, z), \quad (3)$$

one notes that  $F(x, z) = 0$  above the surface,  $z > D(x)$ , since  $V(x, z) \equiv 0$  in this region. Below the surface, the wave function is identically zero, so that the Schrödinger equation

$$-(\hbar^2/2\mu)\nabla^2\psi + V\psi = E\psi$$

or

$$\begin{aligned} V(x, z)\psi(x, z) &= F(x, z) \\ &= E\psi(x, z) + (\hbar^2/2\mu)\nabla^2\psi(x, z) \end{aligned} \quad (4)$$

implies that  $F(x, z) = 0$  also for  $z < D(x)$ . More precisely, since  $\psi(x, z) = 0$  below (and on) the surface, and  $\psi(x, z) \neq 0$  above the surface, the second derivative of  $\psi$  must behave like a Dirac  $\delta$  function at the surface, and Eq. (4) therefore implies that  $F(x, z)$  is of the form

$$F(x, z) = f(x)\delta(z - D(x)), \quad (5)$$

where  $D(x)$  is the surface contour and  $f(x)$  an undetermined function of  $x$ . The combination of Eqs. (2), (3), and (5) results in

$$\begin{aligned} \psi(x, z) &= \Phi_I(x, z) + \int_{-\infty}^{\infty} dx' \int_{-\infty}^{\infty} dz' \\ &\quad \times G_0^*(x, z; x', z') f(x') \delta(z' - D(x')), \\ \psi(x, z) &= \Phi_I(x, z) + \int_{-\infty}^{\infty} dx' \\ &\quad \times G_0^*(x, z; x', D(x')) f(x'). \end{aligned} \quad (6)$$

Before proceeding further it is useful to examine the one-dimensional analog of this equation,

$$\psi(z) = \Phi_I(z) + \int_{-\infty}^{\infty} dz' G_0^*(z, z') f\delta(z - D). \quad (7)$$

This equation can be solved exactly, and gives

$$\psi(z) = e^{-ikz} - e^{-iD} e^{ik|z-D|}. \quad (8)$$

The wave function vanishes identically for  $z < D$ , and is an incoming plus an outgoing scattered wave for  $z > D$ . Thus Eq. (6) behaves correctly in this simple one-dimensional case.

If the incident wave is a plane wave of the form

$$\Phi_I = e^{+i(k_x^0 x + k_z^0 z)}, \quad (9)$$

then Eq. (6) becomes

$$\begin{aligned} \psi(x, z) &= e^{+i(k_x^0 x + k_z^0 z)} \\ &\quad + \int_{-\infty}^{\infty} dx' G_0(x, z, x', D^0(x')) f(x'), \end{aligned} \quad (10)$$

where, for convenience,  $D(x')$  has been replaced by  $D^0(x')$ . For the results to be exact

$$D^0(x') \equiv D(x), \quad (11)$$

but other approximations are possible.

For a periodic lattice the integral in (10) can be collapsed to an integral over the unit cell times a phase factor for the position of each unit cell:

$$\begin{aligned} \psi(x, z) &= e^{+i(k_x^0 x + k_z^0 z)} + \int_{-a/2}^{a/2} dx' \\ &\quad \times \sum_{n=-\infty}^{+\infty} G_0^*(x, z, x' - na, D^0(x')) e^{-ik_z^0 na} f(x'), \end{aligned} \quad (12)$$

where  $a$  is the unit-cell dimension. It is now convenient to define a modified Green's function by

$$\begin{aligned} G_1(x, z, x', z') &= \sum_{n=-\infty}^{\infty} G_0^*(x, z, x' - na, z') e^{-ik_x^0 na}. \end{aligned} \quad (13)$$

Using the integral form of the free-particle Green's function

$$G_0^*(x, z, x', z') = \lim_{\epsilon \rightarrow 0^+} \frac{2M}{\hbar^2} \int_{-\infty}^{\infty} dk_z \int_{-\infty}^{\infty} dk_x \frac{\exp\{i[k_x(z - z') + k_x(x - x')]\}}{k_x^2 + k_z^2 + i\epsilon - (k_x^2 + k_z^2)}, \quad (14)$$

and defining  $k$  by

$$k^2 = k_x^0{}^2 + k_z^0{}^2, \quad (15)$$

yields

$$G_1 = \lim_{\epsilon \rightarrow 0^+} \frac{2M}{\hbar^2} \int dk_z \int dk_x \frac{\exp\{i[k_z(z-z') + k_x(x-x')]\}}{k_x^0{}^2 + k_z^0{}^2 + i\epsilon - (k_x^2 + k_z^2)} \sum_{n=-\infty}^{\infty} \exp[i(k_x - k_x^0)na]. \quad (16)$$

The sum is a  $\delta$  function which gives the diffraction conditions:

$$G_1 = \lim_{\epsilon \rightarrow 0^+} \frac{2M}{\hbar^2} \int dk_z \int dk_x \frac{\exp\{i[k_z(z-z') + k_x(x-x')]\}}{k^2 + i\epsilon - (k_x^2 + k_z^2)} \sum_{l=-\infty}^{\infty} \delta\left(\frac{(k_x - k_x^0)a}{2\pi} - l\right). \quad (17)$$

Performing the integrations

$$G_1 = -\frac{4\pi^2 M i}{a\hbar^2} \sum_l \frac{\exp\{i[(2\pi/a)l + k_x^0](x-x') + |z-z'| \{k^2 - [(2\pi/a)l + k_x^0]^2\}^{1/2}\}}{\{k^2 - [(2\pi/a)l + k_x^0]^2\}^{1/2}}, \quad (18)$$

defining  $\theta_l$  by

$$\theta_l = \arcsin\left(\frac{k_x^0 + 2\pi l/a}{k}\right), \quad (19)$$

and noting that  $\theta_l$  is the angle for  $l$ th-order diffraction peak, gives the following result for the modified Green's function:

$$G_1 = -\frac{4\pi^2 M i}{ak\hbar^2} \sum_{l=-\infty}^{\infty} \frac{\exp\{ik[\sin\theta_l(x-x') + \cos\theta_l|z-z'|]\}}{\cos\theta_l}. \quad (20)$$

Substituting this expression for the modified Green's function into (12) gives

$$\psi(x, z) = e^{i(k_x^0 x + k_z^0 z)} - \frac{4\pi^2 M i}{ak\hbar^2} \sum_{l=-\infty}^{\infty} \int_{a/2}^{a/2} \frac{f(x') \exp\{ik[\sin\theta_l(x-x') + \cos\theta_l|z-D^0(x')|]\}}{\cos\theta_l}. \quad (21)$$

One now expands  $f(x')$  in a Fourier series,

$$f(x') = \frac{k\hbar^2}{4\pi M i} \sum_{n=-\infty}^{\infty} C_n e^{i[(2\pi/a)n + k_x^0]x'}. \quad (22)$$

Combining (21) and (22) gives

$$\psi(x, z) = e^{i(k_x^0 x + k_z^0 z)} - \sum_{n=-\infty}^{\infty} \sum_{l=-\infty}^{\infty} \frac{C_n e^{ik \sin\theta_l x}}{\cos\theta_l} \int_{-1/2}^{1/2} d(x'/a) \exp\{i[2\pi(n-l)(x'/a) + k \cos\theta_l |z - D^0(x')|]\}. \quad (23)$$

$D(x)$  is now chosen to be sinusoidal

$$D^0(x) = D(x) = ha \sin(2kx/a), \quad (24)$$

and the coefficients  $\{C_n\}$  that define the function  $f(x)$  in Eq. (22) are determined by requiring that  $\psi(x, z) \equiv 0$  for  $z < -ha$ ; from Eq. (23) one sees that this condition implies

$$0 = e^{i(k_x^0 x + k_z^0 z)} - \sum_{l,n} \frac{C_n \exp[ik(x \sin\theta_l - z \cos\theta_l)]}{\cos\theta_l} \int_{-1/2}^{1/2} d(x'/a) \exp\{i[2\pi(n-l)(x'/a) + hka \cos\theta_l \sin(2\pi x'/a)]\}. \quad (25)$$

The integral in Eq. (25) is a Bessel function, so the equation for the  $\{C_n\}$  becomes

$$e^{i(k_x^0 x + k_z^0 z)} = \sum_{l,n} \frac{C_n e^{i(k_x^l x + k_z^l z)}}{\cos\theta_l} J_{n-l}(hka \cos\theta_l), \quad (26)$$

where

$$k_x^l \equiv k \sin\theta_l,$$

$$k_z^l \equiv -k \cos\theta_l.$$

Taking Fourier components of Eq. (26), and noting

that  $k_x^{l=0} = k_x^0$ ,

$$(\cos\theta_l) \delta_{l,0} e^{i(k_x^0 x - k_z^0 z)} = \sum_n C_n J_{n-l}(hka \cos\theta_l). \quad (27)$$

Since  $\theta_l = 0$  and  $k_z^{l=0} = +k_z^0$ , the set of linear equations which determine the coefficients  $\{C_n\}$  is

$$\cos\theta_l \delta_{l,0} = \sum_n C_n J_{n-l}(hka \cos\theta_l). \quad (28)$$

With the coefficients  $\{C_n\}$  determined by Eq. (28), the wave function is now completely determined

via Eq. (23), and one only needs to look in the asymptotic region to find the scattering amplitude. Above the surface,  $z > ha$ , the wave function of Eq. (23) becomes

$$\begin{aligned} \psi(x, z) = & \Phi_I - \sum_{n, l} \frac{C_n e^{i(k_x^l x + k_z^l z)}}{\cos \theta_l} \int_{-1/2}^{1/2} d(x'/a) \\ & \times \exp \{ i [ 2\pi(n-l)(x'/a) \\ & - hka \cos \theta_l \sin(2\pi x'/a) ] \}. \end{aligned} \quad (29)$$

The integral is again a Bessel function, and since  $x = r \sin \theta$  and  $z = r \cos \theta$ , this becomes

$$\begin{aligned} \psi(x, z) \equiv & \psi(r, \theta) \\ = & \Phi_I - \sum_{l, n} \frac{C_n e^{ikr \cos(\theta_l - \theta)}}{\cos \theta_l} J_{l-n}(hka \cos \theta_l). \end{aligned} \quad (30)$$

In the limit  $r \rightarrow \infty$  it is not hard to show that

$$\begin{aligned} \lim_{r \rightarrow \infty} e^{ikr \cos(\theta_l - \theta)} &= e^{ikr(2\pi/ikr)^{1/2} \delta(\theta - \theta_l)} \\ &= e^{ikr(2\pi/ikr)^{1/2} \cos \theta_l \delta(\sin \theta - \sin \theta_l)}, \end{aligned} \quad (31)$$

so that in the asymptotic region the wave function in Eq. (30) becomes

$$\psi(r, \theta) \sim \Phi_I + (e^{ikr/r^{1/2}}) f(\theta), \quad (32)$$

where the scattering amplitude  $f(\theta)$  is

$$f(\theta) = -e^{-i\pi/4} \left( \frac{2\pi}{k} \right)^{1/2} \sum_{l=-\infty}^{\infty} S_l \delta(\sin \theta - \sin \theta_l), \quad (33)$$

with the S-matrix elements given by

$$S_l = \sum_{n=-\infty}^{\infty} C_n J_{l-n}(hka \cos \theta_l). \quad (34)$$

Note that the S-matrix elements have been defined so that the normalization conditions is

$$\sum_{l=-\infty}^{\infty} |S_l|^2 \frac{\cos \theta_l}{\cos \theta_l} = 1. \quad (35)$$

In summary, the coefficients  $\{C_n\}$  are determined by solving the set of linear equations Eq. (28), and the scattering amplitude is then given by Eqs. (33) and (34).

Beeby<sup>8</sup> has used a different procedure to calculate the scattering pattern from a sinusoidal hard wall. An equation similar to Eq. (5) is used, except that the contour  $D^0(x)$  is assumed to be somewhere beneath the surface, and it is assumed to be sufficient to satisfy the boundary condition,  $\psi = 0$ , along the surface. It would be interesting to see how the results of this procedure compare with Eqs. (26) and (27). To do so, a sinusoidal hard wall will again be assumed, and  $D^0(x)$  will be taken to be

$$D^0(x) \equiv y - \text{where } y \text{ is below the surface.} \quad (36)$$

A procedure similar to those used to derive Eq.

(27) shows that the wave function is given by

$$\psi(x, z) = e^{i(k_x^0 x + k_z^0 z)} + \sum_n \frac{C_n e^{i(k_n^x x + k_n^z z)}}{\cos \theta_n}, \quad (37)$$

with the coefficients determined by

$$-J_{-l}(ahk_z^0) = \sum_n \frac{C_n J_{n-l}(ahk \cos \theta_n)}{\cos \theta_n}. \quad (38)$$

The solutions of Eqs. (37) and (38) should be compared to the solution of Eqs. (28) and (29). Unless the surface is flat (i. e.,  $h=0$ ) the solutions are different even at distances far above the surface. This means that  $\psi = 0$  on the surface is a necessary but not a sufficient condition for the exact solution.

## RESULTS AND DISCUSSION

The scattering from this sinusoidal hard wall may be calculated by first solving Eq. (28) for the coefficients  $C_n$ , and then inserting them into Eq. (29). Equation (28) is infinite dimensional, and a finite-dimensional approximation must be used.

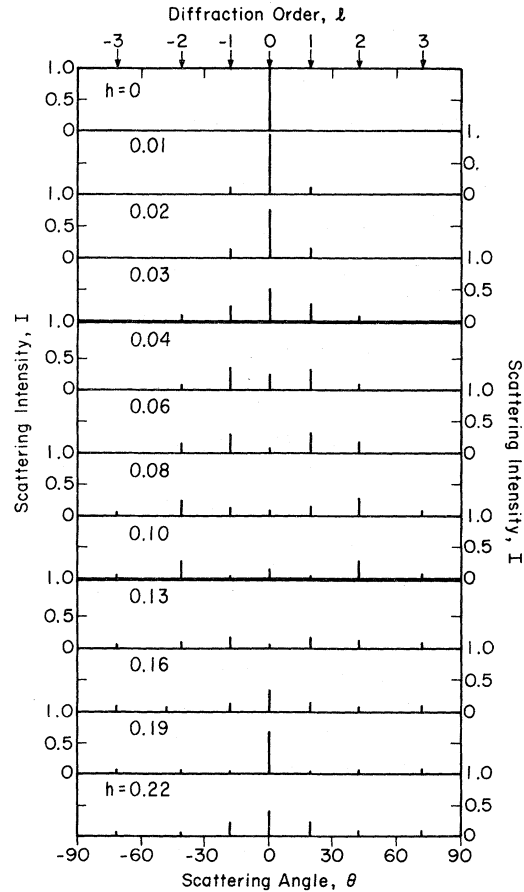


FIG. 1. Scattering intensity as a function of angle for a wave at normal incidence, with  $ka=40$  and  $h$ , as indicated on the figure.

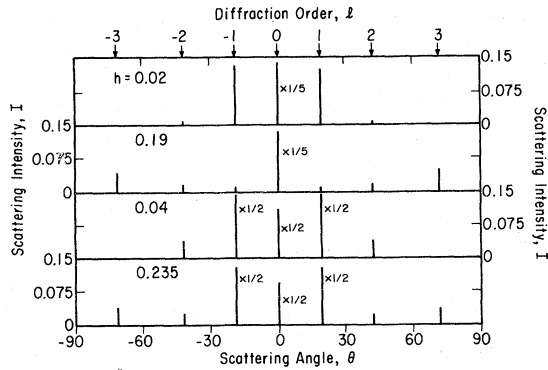


FIG. 2. Magnified comparison of the superficially similar cases in Fig. 1,  $ka=40$ ,  $\theta_I=0$ , and  $h$  is as indicated in the figure.

It was decided to consider only those coefficients  $C_n$  whose index  $n$  was less than a predetermined number  $N$  in absolute value.  $N$  was then increased until the intensity  $I_l$ , given by

$$I_l \equiv |S_l|^2, \quad (39)$$

converged to four significant figures for all of the allowed beams (i. e., all those with  $|2\pi l/ka| > 1$ ). Empirically, the required value of  $N$  can be estimated from

$$N \approx ka/2\pi + 3 + kah. \quad (40)$$

In the calculations  $N$  was always taken to be larger than this to verify convergence. All of the calculations presented here are for normal incidence. There are two net parameters in the model; roughness  $h$  and dimensionless incident  $k$  vector  $ka$ .

Figure 1 shows scattering patterns calculated for a typical value of the dimensionless  $k$  vector  $ka$  and various values of the roughness  $h$ . Qualitatively, they are similar to the coupled channel calculations of Tschuda<sup>9</sup> and Wolken,<sup>10</sup> and the semiclassical calculations of Levi,<sup>11</sup> Masel,<sup>12</sup> and Doll,<sup>13</sup> as well as the scattering data, but do not agree even qualitatively with the single scattering calculations of Goodman<sup>6</sup> and the structured surface calculations of Beeby.<sup>8</sup>

The scattering patterns in the top part of the figure ( $h < 0.04$ ) are for relatively smooth surfaces. They are specularly dominated. The intensity is largest at the specular peak, and decreases substantially as one moves to the higher-order diffraction features. Even so, if  $h$  is not zero, all of the diffraction features will have a nonzero intensity. Increasing the roughness causes the intensity of all of these diffraction features to increase at the expense of the specular. Eventually the specular peak will have a smaller intensity than some of the diffraction features and a "rainbowlike" pattern such as those shown in the middle

part of Fig. 1 ( $0.03 < h < 0.13$ ) is formed. A "rainbow" pattern is one with maxima in the intensity as a function of diffraction order, which are dispersed away from the specular beam. The "rainbow angles" are defined to coincide with the intensity maxima. Between the rainbow angles the intensity is decreased and seems, in these hard-wall cases, to have a doubly periodic structure, similar to that predicted by Levi *et al.*<sup>7</sup> The effect of increased roughness is to move the rainbow angles out and increase the double periodicity between the rainbow angles.

At very high roughness, such as those seen in the bottom of Fig. 1 ( $h > 0.13$ ), just the opposite begins to happen. Increased roughness makes the rainbow angles appear to move in again, and wipes out the double periodicity. Superficially, some of the scattering patterns from very rough surfaces look much the same as those from very smooth ones.

A closer comparison (Fig. 2) shows that the scattering patterns are different. On the smooth surfaces the higher-order features are strongly attenuated, but on the rough surfaces they are clearly evident. They form a weak rainbow pattern, which is superimposed on the strong rainbow or specularly dominated pattern of the lower-order features. This is highly suggestive of multiple scattering and indeed, in a semiclassical approximation, multiple scattering occurs when  $h \geq 0.13$ .

Figure 3 shows scattering patterns calculated for an intermediate roughness and various  $k$  vectors. These scattering patterns are fairly similar. All of the patterns show a rainbowlike structure, and the rainbow angles are all at about the same place. A doubly periodic intensity profile for those peaks between the rainbow angles is seen in all of the patterns. The only difference between the various patterns seems to be that with a higher  $k$  vector the total intensity must be spread over a greater number of peaks, and so each peak has a

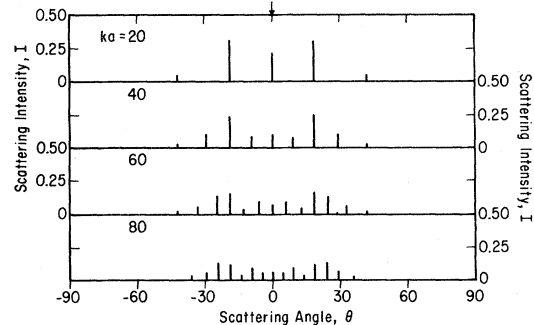


FIG. 3. Effect of incident  $k$  vector on the scattering patterns with  $h=0.04$  and  $\theta_I=0$ .

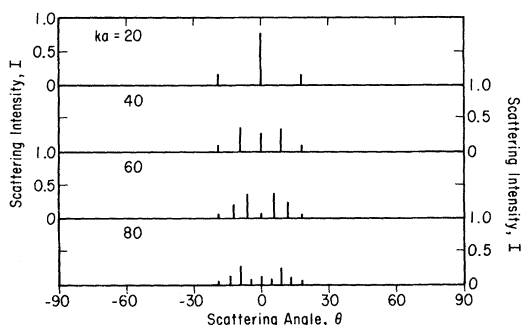


FIG. 4. Effect of incident  $k$  vector on the scattering patterns with  $h=0.02$  and  $\theta_I=0$ .

lower intensity. Note that this effect occurs naturally from Eqs. (28) and (29), and it was not necessary to scale the coefficients to force normalization. Indeed the normalization condition

$$\sum_l \frac{I_l}{(\cos\theta_l)} = \frac{1}{(\cos\theta_I)}, \quad (41)$$

$$|l| \geq ka/2\pi,$$

was satisfied to less than 0.1% for all of the cases studied.

Figure 4 shows scattering patterns calculated for various  $k$  vectors and a relatively smooth surface. The scattering pattern for the lowest  $k$  vector are specularly dominated just like those in Fig. 1, but the higher-energy patterns are rainbows like those in Fig. 2. The rainbow angles are all at about the same place independent of the  $k$  vector. One should note that for the smallest  $k$  vector there is no allowed peak in the region where the rainbow is seen at the other energies. Empirically, no matter how rough the surface may be, if there are no allowed peaks in the neighborhood of the rainbow angle, the scattering pattern is specularly dominated in a manner similar to those in the top part of Fig. 1.

Figure 5 is a plot of the intensities of the specular and first- and second-order diffraction beams as a function of the incident  $k$  vector with a roughness of 0.10. In the region where

$$ka \leq 2\pi$$

only the specular beam can propagate and so the specular intensity is unity, and all of the other beams have near zero intensity. At higher  $k$  vectors, other beams are seen.

Once a beam begins to appear, it increases rapidly in intensity, slowly decays, and then shows an oscillatory behavior at higher values of  $k$ . The rapid increase occurs only for very rough surfaces. With this particular roughness, the rainbow angles are about  $\pm 70^\circ$ , and so the intensity increases

rapidly with energy as the beam emerges from the surface and sweeps past the rainbow angle. With a lower roughness, the rainbow angles are farther away from  $90^\circ$ , and so the intensity increases more gently. Still, as more and more allowed beams emerge, there is a general decrease in the magnitude of the allowed beams throughout the intensity profile.

Using a semiclassical model,<sup>12</sup> it is easy to show that for large  $k$  vectors the intensities of the various peaks at normal incidence follow<sup>16</sup>

$$I_l = J_1^2(2hka). \quad (42)$$

One would expect peaks whenever

$$2hka = [n + \frac{1}{2} + \frac{1}{4}(-1)^{l+1}]\pi,$$

and valleys in between. This general trend is reproduced by these calculations, but at present a more detailed comparison with the semiclassical formulation has not been completed.

#### CONCLUSIONS

Equations (28) and (29) are an exact quantum description of the scattering pattern from a sinusoidal hard wall. The condition that the wave function  $\psi$  goes to zero everywhere below the surface is satisfied and the solution is unique. The "boundary condition" that  $\psi$  goes to zero only on the surface does not, by itself, produce the correct solution.

Equation (28), though, is an infinite-dimensional matrix equation in the coefficients  $C_n$ , and must be solved in a finite-dimensional limit. This approximation, however, seems to introduce little error if  $N$  is taken to be equal to or larger than the value given in Eq. (40). In all cases the normalization condition, Eq. (41), is satisfied to less than 0.1%.

The results of the calculations show either rainbow or specular patterns according to the incident  $k$  vector and surface roughness in qualitative agreement with semiclassical calculations of

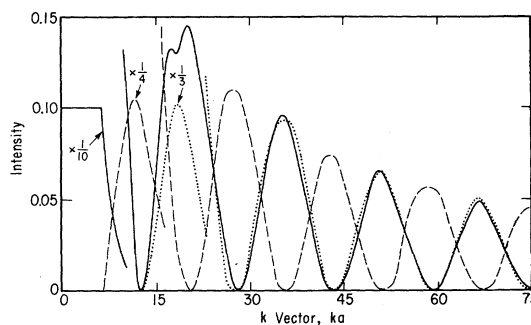


FIG. 5. Intensity of the specular (solid line) and the first (dashed line) and second (dotted line) order diffraction features as a function of incident  $k$  vector with  $h=0.10$  and  $\theta_I=0$ .

Masel,<sup>12</sup> Doll,<sup>13</sup> and Levi,<sup>11</sup> and the coupled-channel expansions of Wolken<sup>10</sup> and Tschuda.<sup>9</sup> The calculations of Goodman<sup>6</sup> and Beeby<sup>8</sup> do not show these qualitative trends.

#### ACKNOWLEDGMENTS

This work has been supported by AFOSR Grant No. 72-2218 and NSF Grant GP-4509X. Computations were carried out on a Datacraft 6024/4 minicomputer funded by NSF Grant No. GP-39317. One of us (W. H. M.) acknowledges support from a Camille and Henry Dreyfus Teacher-Scholar Grant. We also acknowledge helpful discussions with K. Miller and C. Schwartz.

*Note added in proof.* Equations (28) and (34) were derived for a sinusoidal hard wall. For a more general periodic hard wall of the form  $D(x'/a)$ , the equations corresponding to (28) and (34) are

$$\cos\theta_l \delta_{l,0} = \sum_{n=-\infty}^{\infty} C_n H(n-l, ka \cos\theta_l) \quad (28a)$$

and

$$S_l = \sum_{n=-\infty}^{\infty} C_n H(l-n, ka \cos\theta_l), \quad (34a)$$

with

$$H(m, Y) = \int_{-1/2}^{1/2} d\left(\frac{x'}{a}\right) e^{i[2\pi(m)(x'/a) + YD(x'/a)]}.$$

Scattering from periodic arrays is important in optical, acoustic, and wave guide theory. Much of this work has been based on the separable plane-wave representation first used by Rayleigh.<sup>17</sup> It is now known that the Rayleigh solution is not correct for large values of the surface amplitude,  $h$ .<sup>18,19</sup> The solution presented here appears to extend exact calculations to larger surface amplitudes and to be more convenient to apply than the most recent results.<sup>20,21</sup> The work cited here<sup>18-21</sup> confirms our finding that the complete solution is not separable in  $x$  and  $y$  within the region of the scattering surface.

- <sup>1</sup>I. Esterman and O. Stern, *Z. Phys.* **61**, 95 (1930).
- <sup>2</sup>W. H. Weinberg and R. P. Merrill, *Phys. Rev. Lett.* **25**, 1198 (1970).
- <sup>3</sup>D. V. Tendulkar and R. E. Stickney, *Surf. Sci.* **40**, 405 (1973).
- <sup>4</sup>A. G. Stoll, Jr., D. L. Smith, and R. P. Merrill, *J. Chem. Phys.* **54**, 163 (1971).
- <sup>5</sup>J. E. Lennard-Jones and A. F. Devonshire, *Proc. R. Soc. Lond. A* **158** (1937).
- <sup>6</sup>N. Cabrea, U. Celli, F. O. Goodman, and B. Mason, *Surf. Sci.* **19**, 67 (1970).
- <sup>7</sup>J. L. Beeby, *J. Phys. C* **5**, 3438 (1972); **5**, 3457 (1972).
- <sup>8</sup>J. L. Beeby, *J. Phys. C* **6**, 1229 (1973).
- <sup>9</sup>A. Tschuda, *Surf. Sci.* **46**, 611 (1974).
- <sup>10</sup>G. Wolken, *J. Chem. Phys.* **58**, 3047 (1973).
- <sup>11</sup>U. Garibaldi, A. C. Levi, B. Spadacini, and C. E. Tommei (unpublished); *Surf. Sci.* **38**, 269 (1973); G. Boato, P. Cantini, U. Garibaldi, A. C. Levi, L. Mat-

- tera, R. Spadacini, and G. E. Tommei, *J. Phys. C* **6**, L394 (1973).
- <sup>12</sup>R. I. Masel, R. P. Merrill, and W. H. Miller, *Surf. Sci.* **46**, 681 (1974); *J. Chem. Phys.* (to be published).
- <sup>13</sup>J. Doll, *J. Chem. Phys.* **3**, 257 (1974); *ibid.* (to be published); J. Doll and A. S. Adelman (unpublished).
- <sup>14</sup>W. H. Miller, *Adv. Chem. Phys.* **25**, 69 (1974).
- <sup>15</sup>B. A. Lippman and J. Schwinger, *Phys. Rev.* **79**, 469 (1950).
- <sup>16</sup>R. I. Masel, R. P. Merrill, and W. H. Miller (unpublished).
- <sup>17</sup>J. W. Strutt Baron Rayleigh, *Proc. R. Soc. A* **79**, 399 (1907).
- <sup>18</sup>R. F. Millar, *Proc. Camb. Philos. Soc.* **69**, 217 (1971).
- <sup>19</sup>Reference 18, **65**, 773 (1969).
- <sup>20</sup>I. L. Uretsky, *Ann. Phys. (N.Y.)* **33**, 400 (1965).
- <sup>21</sup>P. C. Waterman, *J. Acoust. Soc. Am.* **57**, 792 (1975).